GPS TOOLBOX

An open-source software package for Precise Point Positioning: raPPPid

Marcus Franz Glaner[1] · Robert Weber[1]

Abstract

Precise Point Positioning (PPP) has proven to be a powerful GNSS positioning method used for various scientific and commercial applications nowadays. We present a flexible and user-friendly software package named raPPPid suitable for processing single to triple-frequency GNSS observations in various PPP approaches (e.g., ionospheric-free linear combination, uncombined model), available under https://github.com/TUW-VieVS/raPPPid. To tune the PPP procedure, the user can select from many satellite products, models, options, and parameters. This way, the software raPPPid can handle high-to-low quality observation data ranging from geodetic equipment to smartphones. Despite significant improvements, the convergence time of PPP is still a major topic in scientific research. raPPPid is specially designed to reduce the convergence period with diverse implemented approaches, such as PPP-AR or ionospheric pseudo-observations, and to offer the user multiple plots and statistics to analyze this critical period. Typically, raPPPid achieves coordinate convergence times of around 1 min or below with high-quality observations and ambiguity fixing. With smartphone data and a simplified PPP approach, a 2D position accuracy at the one-meter level or below is accomplished after two to three minutes.

Introduction

Since Malys and Jensen (1990), Héroux and Kouba (1995), and Zumberge et al. (1997) introduced the concept, Precise Point Positioning (PPP) has become a well-established technique for determining the user's position and other valuable parameters like atmospheric delays (Kouba et al. 2017). Thanks to the continuous development of GNSS constellations, PPP typically utilizes observations from multiple GNSS nowadays, improving its performance in all regards (Tegedor et al. 2014; Pan et al. 2017; An et al. 2020). Furthermore, researchers investigate observation models handling three GNSS frequencies (Geng and Bock 2013; Pan et al. 2019; Naciri 2021). Additionally, PPP with integer ambiguity resolution (PPP-AR) has proven as an effective method for reducing or possibly eliminating the convergence time to centimeter-level accuracy (Ge et al. 2008; Teunissen 2020). Due to its characteristics and flexibility, PPP faces a promising future. However, the convergence time of PPP is still a central topic in scientific research and its limiting factor compared to other relative positioning methods (Choy et al. 2017). In the last years, several open-source PPP software packages have become available: RTKLIB (Takasu 2010, 2012), GAMP (Zhou et al. 2018), PPPH (Bahadur and Nohutcu 2018), PRIDE PPP-AR (Geng et al. 2019), MG-APP (Xiao et al. 2020), PPPLib (Chen and Chang 2021), and SUPREME (Zhao et al. 2021). Each software package offers its own advantages and different features. Note that user-friendliness and documentation vary considerably, complicating the installation and first steps.

✉ Marcus Franz Glaner
  marcus.glaner@geo.tuwien.ac.at

1   Department of Geodesy and Geoinformation, Research Division Higher Geodesy, TU Wien, 1040 Vienna, Austria

The Vienna VLBI and Satellite Software (VieVS) offers various software packages for VLBI applications (Böhm et al. 2018), ionosphere models (Magnet 2019; Boisits et al. 2020), and a tropospheric ray-tracing package (Hofmeister and Böhm 2017). In the following, we introduce a MATLAB PPP software named raPPPid — the PPP module of VieVS (VieVS PPP). Contrary to most other PPP software, raPPPid supports PPP-AR for GPS, Galileo, and Beidou with various satellite products available and shows outstanding user-friendliness thanks to its graphical user interface (GUI) and documentation (e.g., wiki). Furthermore, raPPPid achieves remarkable convergence times and can handle high-quality to low-cost GNSS observations due to a flexible program structure, various options, and highly adaptable processing settings. For example, users can directly define a weighting function for the observations in the GUI. VieVS PPP accepts the most common file format standards of the GNSS community (e.g., SINEX BIAS, ORBEX) and supports parallel processing of multiple observation files. The processing results are available in various output formats. Finally, the user can choose from an extensive plot section to illustrate the results, convergence period, quality of the observations and models, and satellite geometry. The figures presented in this article are only an excerpt of the graphical capabilities offered by raPPPid.

The following section introduces the basic workflow and general program structure of raPPPid. The third section presents the implemented PPP models. The fourth and fifth sections show processing results for high-quality data and smartphones, respectively. Our conclusions are drawn in the final section. In addition to this article, the raPPPid wiki (https://vievswiki.geo.tuwien.ac.at/en/raPPPid) explains all options and settings provided in the GUI, and Glaner (2022) presents more theoretical background and results achieved with raPPPid. Furthermore, various publications document applications of raPPPid (Boisits et al. 2020; Glaner and Weber 2021; Hohensinn et al. 2022; Aichinger-Rosenberger et al. 2023).

Program structure

The MATLAB software package of raPPPid can process up to three frequencies from all four globally working GNSS (GPS, GLONASS, Galileo, and BeiDou) in various PPP models presented in the next section. The main characteristics and features are the following:

- The program design allows combining all GNSS and signals, processing different frequencies for each GNSS, and handling static and kinematic observation data with any interval.

- User-friendliness due to a straightforward GUI and a wiki providing processing examples and detailed descriptions
- Automatic download of input data (e.g., a large number of satellite products and models).
- Support of present GNSS file formats (e.g., ORBEX) and self-explanatory output data.
- Numerous processing options and features are available. For example, several quality checks of the observations (e.g., cycle slip detectors) and a wide range of atmospheric corrections.
- Quasi-real-time processing using stream archives or real-time correction streams recorded with the BKG Ntrip Client (BNC).
- Batch processing of observation files optionally using parallelization (MATLAB parfor loop). The processing name and manually selected input data can be designed adaptively (e.g., depending on the day to process).
- A remarkable amount and variety of plots. So-called multi-plots are specifically designed for analyzing the convergence period.
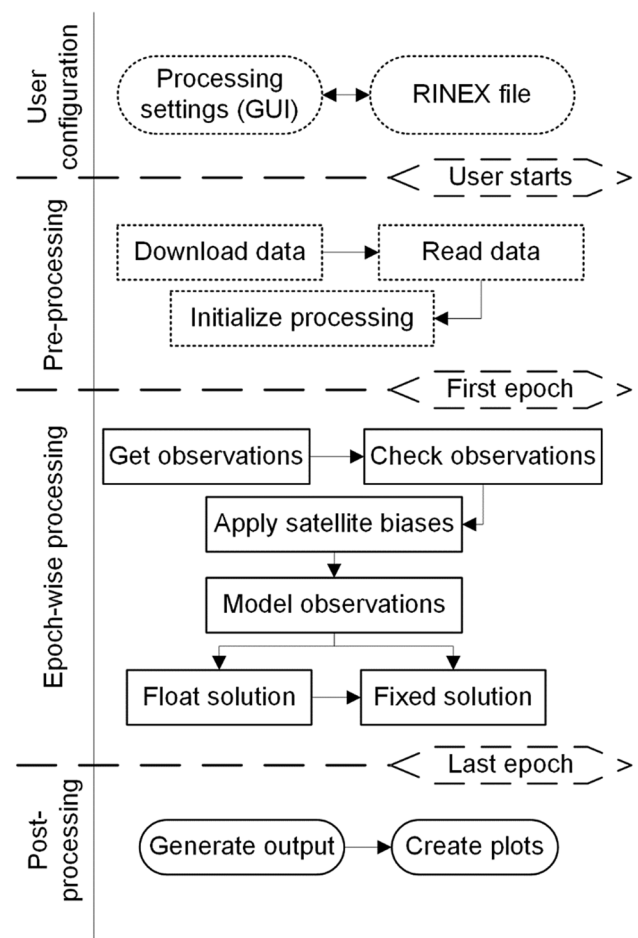

Fig. 1 Overview of the workflow of raPPPid

Figure 1 presents the main workflow of raPPPid. The processing can be divided into four major steps. First, the user has to select a RINEX observation file and configure the processing settings in the GUI. After the user starts the processing from the GUI, raPPPid performs the calculations automatically. All needed input data is downloaded and read in during the pre-processing phase. Then, the epoch-wise processing runs as a loop over the selected epochs of the RINEX observation file. Note that it is possible to insert resets of the PPP solution in specific epochs useful to study the convergence behavior (e.g., multi-plots). When raPPPid reaches the last epoch to process, the epoch-wise calculation of the PPP solution is completed, and raPPPid creates the output data used for visualization.

Table 1 shows an overview of the program-internal order of GNSS and frequencies. The order of GNSS is relevant, for example, for estimating the receiver clock offsets. Furthermore, Table 1 presents the used GNSS acronyms (e.g., variable names) and the internal satellite numbering, which is used additionally to common satellite naming (e.g., G01 or E32). A multiple of a hundred is added to the satellite's PRN depending on the GNSS satellite to obtain the raPPPid internal satellite number. This strategy allows storing satellite-specific data in a specific epoch in vectors and saving the data from the whole processing in matrices.

PPP models

The PPP models implemented in raPPPid mainly differentiate in the handling of the ionospheric delay. The two main options are the conventional PPP model based on two signal frequencies for building the ionospheric-free linear combination (IF LC) and the uncombined model managing any number of frequencies (Schönemann 2013). Furthermore, VieVS PPP can process a single 3-frequency IF LC built with the formulas provided by Pan et al. (2019). For simulated data, raPPPid also offers the possibility to ignore the ionospheric delay completely or correct the raw GNSS observations with an ionosphere model. Note that Inter-frequency clock biases (IFCBs) are not considered currently.

$$P_i = \rho + c\left(dt_R - dt^S\right) + dTrop + dIono_i + B_{R,i} - B_i^S + \varepsilon \tag{1}$$

$$L_i = \rho + c\left(dt_R - dt^S\right) + dTrop - dIono_i + \left(N_i + b_{R,i} - b_i^S\right)\lambda_i + \varepsilon \tag{2}$$

These two principal PPP models are introduced starting from the GNSS observation equations (Teunissen and Montenbruck 2017) presented in units of meters in (1) and (2) for the code observable P_i and phase observable L_i, respectively, on frequency i. No index for the GNSS is included to improve the readability. The geometric distance between the satellite and receiver is denoted as ρ. The receiver clock error dt_R and satellite clock error dt^S are both multiplied by the speed of light c. dTrop and dIono denote the tropospheric and ionospheric delays. Receiver and satellite code hardware delays represented as B_R and B^S, respectively, are converted to the range, and ε includes random and other negligible errors. The ambiguity term of the phase observable comprises the integer term N and carrier phase hardware delays from the receiver b_R and the satellite b^s and is multiplied by the wavelength λ_i.

Fundamentally, PPP relies on precise satellite orbits, clocks, and biases. Therefore, the PPP observation equations presented in the following do not include a satellite orbit error, satellite clock error, or satellite code hardware delays. Furthermore, raPPPid models various error sources, such as the hydrostatic part of the tropospheric delay, relativistic effects, phase wind-up, satellite and receiver phase center offset and variations, deformation of the solid earth surface, group delay variations (GDVs), and ocean loading (Glaner 2022). For the so-called float solution, phase hardware delays originating from the receiver and satellite are lumped together with the integer term of the ambiguity to the float ambiguity, denoted as $\widetilde{N}$ below.

$$P_{IF} = \frac{f_1^2}{f_1^2 - f_2^2}P_1 - \frac{f_2^2}{f_1^2 - f_2^2}P_2 \tag{3}$$

$$L_{IF} = \frac{f_1^2}{f_1^2 - f_2^2}L_1 - \frac{f_2^2}{f_1^2 - f_2^2}L_2 \tag{4}$$

$$P_{IF} = \rho + c\left(dt_R^{GNSS_1} + \delta t_R^g\right) + dTrop^{wet} + \varepsilon \tag{5}$$

$$L_{IF} = \rho + c\left(dt_R^{GNSS_1} + \delta t_R^g\right) + dTrop^{wet} + \widetilde{N}_{IF}\lambda_{IF} + \varepsilon \tag{6}$$

Table 1 Program-internal acronyms, satellite numbering, and order of GNSS and signal frequencies

GNSS	Index	Acronyms	Satellite numbering	Order of signal frequencies
GPS	1	GPS, G	1–99	L1, L2, L5
GLONASS	2	GLO, R	101–199	G1, G2, G3
Galileo	3	GAL, E	201–299	E1, E5a, E5b, E5, E6
BeiDou	4	BDS, C	301–399	B1, B2, B3

The IF LC denoted by the subscript *IF* is built for GNSS signals on two frequencies and the corresponding frequencies f_1 and f_2 with (3) and (4) for the code and phase observable, respectively. This approach eliminates the first-order ionospheric delay and is widely used for PPP by neglecting higher-order terms of the ionosphere (Hadas et al. 2017). Accordingly, this approach is called the conventional PPP model, and (5) and (6) present the corresponding PPP observation equations.

$$P_i = \rho + c\left(dt_R^{GNSS_1} + \delta t_R^g\right) - DCB_{1i} + dTrop^{wet} + \gamma_{1i}dIono_1 + \varepsilon \tag{7}$$

$$L_i = \rho + c\left(dt_R^{GNSS_1} + \delta t_R^g\right) - DCB_{1i} + dTrop^{wet} - \gamma_{1i}dIono_1 + \widetilde{N}_i\lambda_i + \varepsilon \tag{8}$$

The PPP observation equations of the uncombined PPP model are presented in (7) and (8) for the code and phase observation, respectively. The uncombined model is a modern and more direct application of the GNSS observation equations suitable for any number of frequencies. Since the raw measurements are processed, the original observation noise is maintained and not increased through the coefficients of a LC, which is usually beneficial for the convergence time of PPP (Lou et al. 2016; An et al. 2020).

VieVS PPP uses an Iterative Extended Kalman Filter for the float solution to estimate the unknown parameters. Both introduced PPP models determine the receiver's coordinates (implicitly included in ρ), wet tropospheric delay $dTrop^{wet}$, float ambiguities $\widetilde{N}$, receiver clock error $\delta t_R^{GNSS_1}$, and receiver clock offsets δt_R^g. The receiver clock error is estimated for the first processed GNSS (Table 1), usually GPS. Furthermore, a receiver clock offset is added for each additionally processed GNSS. For example, raPPPid estimates the GPS receiver clock error and receiver clock offsets for GLONASS and BeiDou in a GRC processing. In the case of the uncombined model, receiver DCBs (DCB_{1i}) and slant ionospheric delays on the first frequency for each satellite $dIono_1$ are additionally estimated. Thereby, the ratio of the squared frequencies $\gamma_{1i} = f_1^2/f_j^2$ is used for converting ionospheric delays to the first frequency (e.g., from Galileo E5b to E1). Note that raPPPid also allows for correcting receiver DCBs.

$$dIono_{pseudo} = dIono_1 + \varepsilon \tag{9}$$

VieVS PPP optionally allows including ionospheric pseudo-observations in the uncombined model (9), leading to the uncombined model with ionospheric constraint. Therefore, the ionospheric delay on the first frequency is modeled for each satellite with an arbitrary ionosphere model and added as pseudo-observation. In this way, the rank deficiency between the receiver DCBs and the ionospheric delay is removed, leading to uncontaminated estimates. VieVS PPP uses a linear approach for increasing the

variance of the ionospheric pseudo-observations over time (Boisits et al. 2020). This strategy allows raPPPid to optimally integrate ionosphere models and their imperfections into the PPP solution and has proven beneficial regarding the convergence time.

$$\widetilde{N} = \overline{N} + b_R - b^S \tag{10}$$

For integer ambiguity fixing, raPPPid corrects satellite hardware phase delays b^S with a suitable bias product and eliminates the receiver hardware phase delays b_R by choosing a reference satellite for each GNSS and building satellite single differences (SD). Remember that for the float solution, these phase delays were lumped together with the integer term $\overline{N}$ to the float ambiguity $\widetilde{N}$ as indicated in (10). By taking the estimated float ambiguities and the corresponding covariance matrix from the float solution, raPPPid can fix GPS, Galileo, and BeiDou ambiguities to integers and calculate an ambiguity fixed coordinate solution. Apart from that, the float and fixed solution are entirely separated. The fixed coordinates are estimated in a Least-Squares-Adjustment adjustment by introducing the fixed ambiguities as highly weighted pseudo-observations.

In the fixing process of the conventional model, the SD ambiguities of the Wide-Lane (WL) and Narrow-Lane (NL) are resolved consecutively using the Hatch-Melbourne-Wübbena LC and partial ambiguity resolution of the LAMBDA algorithm (Teunissen 1995), respectively (Glaner and Weber 2021). In addition to ambiguity fixing with the conventional model, raPPPid supports an experimental approach for PPP-AR with the uncombined model introduced in Glaner (2022). For this purpose, satellite products allowing integer ambiguity fixing the raw ambiguities model are necessary.

High-quality data

The high-quality GNSS observations of 24 globally distributed IGS MGEX stations recorded with an interval of 1 s on August 1, 2022, are processed with raPPPid (Fig. 2).
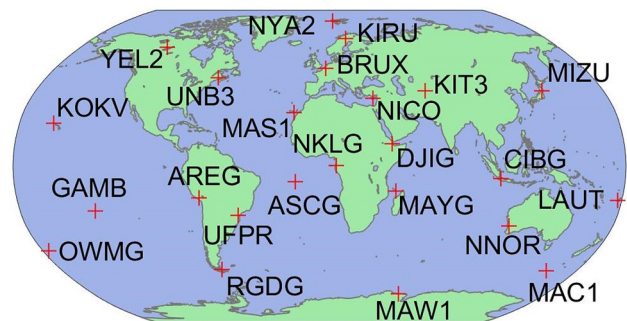

Fig. 2 Distribution of the 24 IGS MGEX stations

These stations were randomly selected to cover the entire globe, but only stations with complete data and daily IGS coordinate estimation were considered eligible. The PPP solution is restarted every 15 min to comprehensively study the convergence behavior, resulting in around 2300 convergence periods. In the following, IGS products are used as a reference to assess the PPP results (e.g., final station coordinates, troposphere product, and final global ionosphere map (GIM)). The convergence time of the float coordinates is defined as the period until the 2D position difference is under the threshold of 10 cm and stays there for the entire remaining processing period. For the fixed solution, convergence is defined as the time to correct fix (TTCF), which is achieved when the 2D position difference of the fixed coordinates stays under the threshold of 5 cm until the remaining processing period.

Table 2 shows an overview of the processing settings. Settings only valid for the uncombined model are written in italic. Furthermore, PPP-AR and ambiguity fixing are only performed with the conventional model (underlined). For this test case, the IGS MGEX satellite products (satellite orbits, attitude, clocks, and biases) generated by the Center of Orbit Determination Europe (CODE) and Wuhan University (WUM) are selected to give an impression of raPPPid's PPP performance. Both analysis centers provide the satellite attitude in the upcoming ORBEX format. CODE MGEX satellite products have proven to perform best regarding ambiguity fixing (Glaner and Weber 2021) and are applied with the corresponding ANTEX file, the conventional model, and

ambiguity fixing. On the other hand, the MGEX satellite products of WUM are used for processing three-frequency observations in the uncombined model with ionospheric constraint. For comparison, a float solution with the conventional model is calculated with WUM products. Typically, the processing time of one processing period on a standard desktop PC ranges from 45 to 60 and 60 to 75 s with the conventional and uncombined model, respectively. The observation ranking (Table 2) decides the processed observations for stations tracking multiple signals on a specific frequency (e.g., GPS C1W is preferred over C1C). Due to the unique characteristics of the BeiDou system and the varying approaches applied by IGS analysis centers, BeiDou proves to be the most challenging system for PPP.
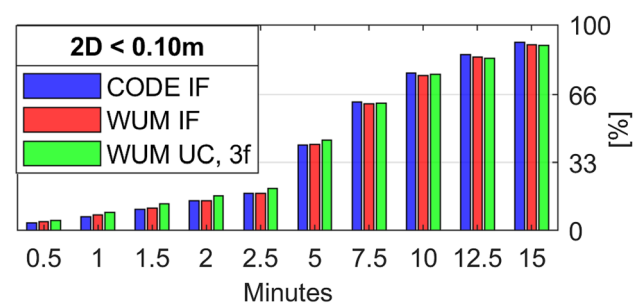

Fig. 3 Bar plot of the float solution convergence. The bars indicate the percentage of convergence periods converged at a specific time after the last reset

Table 2 Overview of processing settings

Software	raPPPid (VieVS PPP)
Stations	24 globally distributed IGS MGEX stations
Day	August 1, 2022 (doy 213)
Observations	GPS: L1+L2+*L5*, GLONASS: G1+G2, Galileo: E1+E5a+*E5b* (GNSS weighting 1: 1.25: 1)
Observation ranking	GPS: WC, GLONASS: PC, Galileo: CQX
Observation interval	1 s, reset of solution: every 15 min
Processing mode	Static, post-processing
Raw observation noise	Code 30 cm, phase 2 mm, *ionosphere 15 cm*
Observation weighting	Elevation weighted, sin($elev$)^2, cutoff angle 3°
Satellite products	CODE or WUM MGEX (orbits, attitude, clocks, and biases)
Ionosphere model	*IGS final, ionospheric constraint used in the first 30 s, the standard deviation is increased to 3 m in that period*
Troposphere model	VMF3+GRAD (Landskron and Böhm 2018a, b), residual zenith wet delay is estimated, process noise 5 mm/√h
Correction models	Phase Wind-Up (Wu et al. 1993), relativistic effects, phase center offsets and variations, solid Earth tides and ocean loading (Petit and Luzum 2010)
Adjustment	Extended Kalman Filter (float solution) and Least-Squares-Adjustment (fixed solution)
Float ambiguities	Constant, zero-difference, cycle-slip detection: dL11-dL2
PPP-AR	Fixing cutoff 10°, the highest satellite is selected as reference satellite, fixing start after 15 s
WL Fixing	Averaging the HMW LC of the last 5 min
NL Fixing	LAMBDA method (Teunissen 1995)

Table 3 Statistics of the float solution applying satellite products from CODE or WUM in the conventional model (IF) or the uncombined model with ionospheric constraint using two or three frequencies (UC2 and UC3, respectively)

	CODE IF	WUM IF	WUM UC2	WUM UC3
Mean convergence time (min)	6.84	6.87	6.84	6.68
No convergence (%)	10.0	11.1	11.4	12.1
Median 3D error after 15 min (cm)	5.86	6.02	6.02	6.29
Median ZTD difference (cm)	1.11	1.13	1.17	1.17

Please note that raPPPid can process BeiDou (Glaner 2022), although its observations are not included in this test case.

Figure 3 shows a bar plot illustrating the convergence behavior of the three processing configurations. The uncombined model with ionospheric constraint (UC) performs better than the conventional model (IF) in the first few minutes. This faster convergence results from using the uncombined approach keeping the raw observation noise, applying an ionosphere model for constraining, and including a third frequency. This improvement would increase in the case of complete three-frequency processing. In this test case, the number of three-frequency observations is considerably reduced because only a limited number of satellites currently emit GPS L5 and raPPPid did not process GLONASS G3 due to missing satellite biases. The difference between the conventional and uncombined approaches decreases over time (Fig. 3). After 10 min, no significant difference between WUM IF and WUM UC is visible. On the other hand, CODE IF and WUM IF perform similarly in the initial period. However, the difference between these two solutions increases over time, and CODE IF outperforms WUM IF after 7.5 min. Most likely, this results from more consistent satellite products.

Table 3 lists the mean convergence times of all cases achieving convergence, the percentage of processing periods without convergence, the median 3D position after 15 min, and the median ZTD difference. For reasons of comparison, Table 3 provides these numbers also for processing two frequencies in the uncombined model with ionospheric constraint. The numbers suggest that the uncombined model performs slightly better in terms of convergence but slightly worse regarding the percentage of not converged cases and the position accuracy after 15 min. Among other things, this can be explained by missing receiver PCOs and PCVs for the third frequency. Currently, raPPPid replaces these with the first frequency values, which are less accurate than calibration values.

Figure 4 illustrates the TTCF's distribution of the complete test case. Grey bars depict the percentage of already correctly fixed convergence periods (cumulative distribution function), and blue bars indicate the percentage of correct fixes happening at this point in time (probability distribution function). Consequently, the height of a specific grey bar
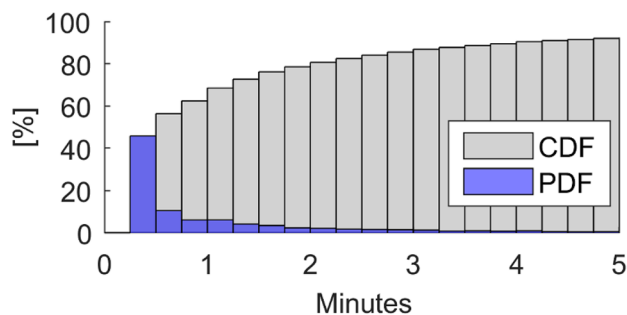

Fig. 4 Distribution of the TTCF during the first 5 min. Grey: Cumulative distribution function (CDF). Blue: probability distribution function (PDF)
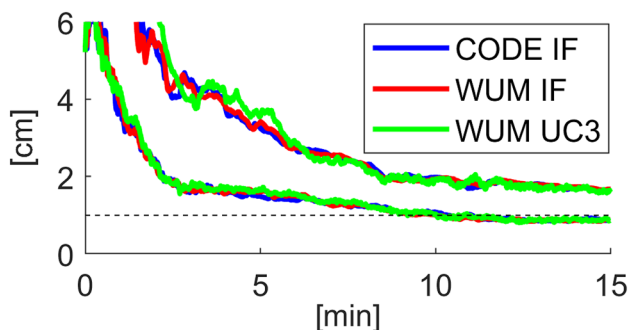

Fig. 5 95% quantile (upper lines) and 68% quantile (lower lines) of the ZTD difference for station UNB3. The black dotted line represents the 1 cm level

equals the height of all blue bars previously or simultaneously in time. The majority of TTCFs takes place within the first minute of processing. The median TTCF (33 s) and mean TTCF (1.36 min) underline this fixing performance. Note that the percentage of cases without a correct fix within 15 min (2.61%) is considerably lower than the corresponding percentage of float convergence periods not reaching convergence (10.0%). The presented numbers underline the significant improvement in convergence behavior through ambiguity fixing, despite applying more strict convergence criteria. Furthermore, the fixed coordinates are more precise than the float coordinates after 15 min (2.81 cm versus 5.86 cm, median 3D position difference).
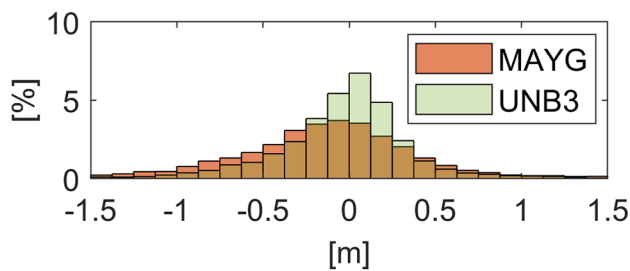
Fig. 6 Histogram of the ionospheric delays' difference for the stations MAYG and UNB3

During the float solution, raPPPid usually estimates the residual zenith wet delay. The total tropospheric delay (ZTD) can then be calculated with the modeled values and compared with the IGS final troposphere product. Figure 5 shows the resulting ZTD difference for station UNB3 (Fredericton, Canada, North America). The choice of satellite product and PPP model does not significantly affect the results, and raPPPid estimates the ZTD at the centimeter level or even below after a convergence time of a few minutes (e.g., five minutes).

The slant ionospheric delay is estimated for each satellite during the PPP solution using the uncombined model with ionospheric constraint and WUM products. The resulting values can be compared with values modeled using the final IGS GIM. Figure 6 shows the resulting histogram of the ionospheric delay differences for the stations MAYG (Dzaoudzi, Mayotte, Africa) and UNB3. The corresponding standard deviations are 0.97 and 0.52 m, respectively. The station MAYG is much closer to the earth equator and, therefore, within an ionospheric more active region, indicating a latitude dependency of the ionospheric delay differences. The corresponding bias is negligible and at the size of a few centimeters (-6 cm and -7 cm, respectively). Since the final IGS GIM usually has an accuracy of 2–8 TECU (Hernández-Pajares et al. 2009), corresponding to a delay error of 0.3–1.3 m on the L1 frequency, and because the presented standard deviations are at this level or below, it is not straightforward to assess the precision. We can expect that the slant ionospheric delay from the PPP solution achieves a higher accuracy than values modeled with a GIM.

Typically, ambiguity fixing significantly reduces the convergence time. The fixed coordinates can jump to their proper values as soon as enough ambiguities are correctly fixed due to calculating the fixed solution with a Least-Squares-Adjustment in raPPPid. However, they also have reached their final precision due to this approach. On the other hand, the float solution converges considerably slower but, thanks to the Kalman Filter, continues increasing the accuracy of the estimated parameters.
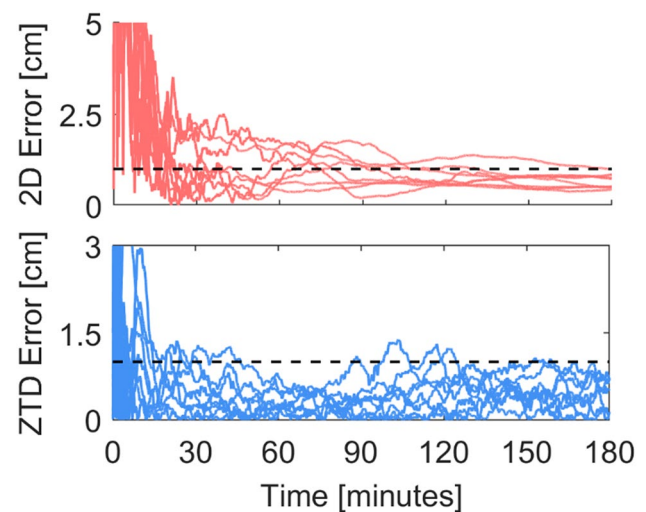

Fig. 7 Long-term behavior of the 2D position difference (top) and the ZTD difference (bottom) for the station AREG (float solution, conventional model, CODE MGEX products, reset every 3 h). The black dashed line represents the one-centimeter level

Figure 7 shows the horizontal position difference (top part) and ZTD difference (bottom part) for the station AREG using the conventional model and CODE MGEX products. For this example, a reset of the solution is performed only every three hours to investigate the long-term behavior of the float solution, leading to eight convergence periods. Please note that the y-axis of the shown 2D position difference and ZTD difference ranges only up to 5 and 3 cm, respectively. The horizontal position difference is around or below the one-centimeter level (black dashed line) after an extensive convergence period of about 30 min. The associated 3D position difference shows similar convergence behavior and is at the size of 1–2 cm. The corresponding ZTD difference with respect to the IGS troposphere product is at the millimeter level, underlined by the corresponding standard deviation of 0.57 cm and bias of 0.35 cm. This example shows that raPPPid can achieve a reasonably stable and precise performance of the long-term float solution on the edge of the physical limits of GNSS.

Smartphone data processing

Since the release of Android 7.0 in 2016, Android users have had access to the raw GNSS measurements of their smartphones (Zangenehnejad and Gao 2021). Therefore, it is possible to use self-developed positioning algorithms to calculate the smartphone position (Shinghal and Bisnath 2021; Wang et al. 2021; Suzuki 2023). However, smartphones are equipped with simple, cost-effective chips and antennas,

typically providing low-quality single-frequency measurements and various challenges (Zhang et al. 2018; Liu et al. 2019; Wanninger and Heßelbarth 2020). Experience showed that the GNSS observations of different smartphone devices behave diversely and unpredictably.

Using thirty minutes of data from two customary smartphone devices (Huawei Nova 5 T and Samsung Galaxy S20FE) recorded on geodetic reference points, we want to demonstrate that raPPPid can smoothly handle such data without going into the details of raw GNSS data from smartphones. Usually, the phase observations of smartphones cannot be easily used in the processing because they behave unpredictably and are affected by cycle slips (e.g., duty cycling) and inconsistencies of the logger applications (Zangenehnejad et al. 2023) if accessible at all. In the presented tests, the recorded RINEX files do not include GLONASS data (Huawei Nova 5 T) or phase observations at all (Samsung Galaxy S20). Figure 8 shows the triple time-differenced

phase observations of four consecutive epochs for a specific GPS, Galileo, and BeiDou satellite (Huawei Nova 5 T). Building the third time difference with high-rate observations typically eliminates nearly all effects and can be used, for example, for cycle slip detection. Clearly, the phase does not show the expected steady behavior, and regular jumps do not allow an estimation of a constant float ambiguity.

Table 4 shows raPPPid's processing options suitable for RINEX files recorded with a smartphone application like the Geo++RINEX Logger. Adapting these settings to a specific smartphone device might improve the results. Generally, weighting the observations based on the SNR performs better than elevation weighting for smartphones, and a basic approach for SNR weighting is used accordingly. The predicted version of the GIOMO model (Magnet 2019) is used for ionospheric pseudo-observations with constant variance in all epochs, stabilizing the estimation of the ionospheric delay and the PPP solution. Furthermore, the complete
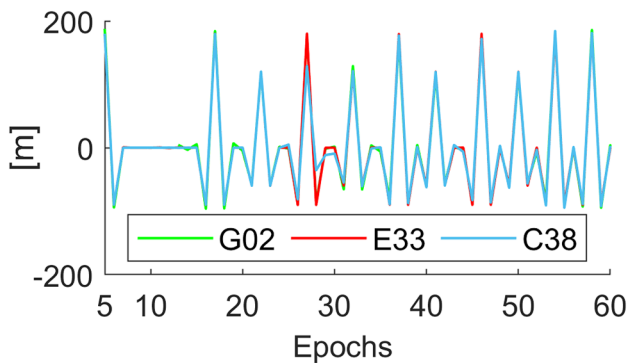

Fig. 8 Triple time-differenced phase observations of the Huawei Nova 5 T for three exemplary satellites. The first minute of the investigated data is shown
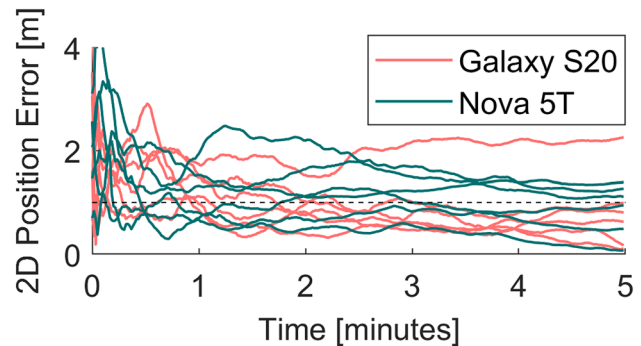

Fig. 9 Convergence behavior of the horizontal position difference for the Samsung Galaxy S20 (red) and Huawei Nova 5 T (green). The black dashed line represents the one-meter level

Table 4 Overview of used smartphone data and processing settings

Devices	Huawei Nova 5 T, Samsung Galaxy S20
	Data recorded with Geo++RINEX Logger
Date	May 25, 2021; September 6, 2022
Period	30 min
Date	RINEX files recorded with Geo+ +RINEX Logger
Observation interval	1 s, reset of solution every 5 min
Satellite orbits, clocks, and biases	CNES stream archive (http://www.ppp-wizard.net/daily.html)
Processing mode	Code only, uncombined model with ionospheric constraint, static, quasi-real-time
Raw observation noise	Code: 3 m, ionospheric pseudo-observations: 2 m
Observation weighting	$10^{-\frac{\max(0;55-SNR)}{20}}$
Ionosphere model	GIOMO predicted (Magnet 2019), constant ionospheric constraint over all epochs
Troposphere model	GPT3 (Landskron and Böhm 2018a, b), hydrostatic and wet delay are modeled
Correction models	Solid Earth tides (Petit and Luzum 2010), relativistic effects
Satellite exclusion criteria	SNR < 20 dB.Hz or elevation < 10°
Data quality checks	Observed minus computed

tropospheric delay is corrected using GPT3 (Landskron and Böhm 2018a, b). Note that due to the applied CNES real-time correction stream data and the selected atmosphere models, the processing framework is capable of real-time.

Figure 9 shows the convergence behavior of the horizontal position for the Galaxy S20 and Nova 5 T. VieVS PPP achieves a 2D position accuracy at the one-meter level or below for both devices after a convergence time of a few minutes. In the case of the Nova 5 T, raPPPid successfully processes single-frequency code observations from all four major GNSS (GPS C1C, GLONASS C1C, Galileo C5Q, and BeiDou C2I) plus GPS L5. On the other hand, solely GPS C1C was processed for the Galaxy S20 because including additional GNSS into the PPP solution introduced a considerable bias in the coordinate estimation (at the several-meter level). The logged observations seem to be influenced by an effect the observation model currently does not cover in multi-GNSS processing.

Figure 10 shows the long-term behavior of the smartphone's topocentric coordinate differences over the entire 30 min for the Galaxy S20 (no resets, ZWD estimated). A stable position at the sub-meter is achieved after convergence, underlined by the RMS values provided in the caption of Fig. 10. The convergence period was excluded from calculating these RMS values (14 min for the height and 3 min for the north and east components). These results achieved with smartphone data collected under static and favorable conditions (e.g., open sky) demonstrate that raPPPid can handle low-cost data from smartphones.

Summary

We have introduced a user-friendly MATLAB PPP software package named raPPPid (also known as VieVS PPP, available under https://github.com/TUW-VieVS/raPPPid). The corresponding wiki (https://vievswiki.geo.tuwien.ac.at/en/raPPPid) provides details on the GUI, models, and
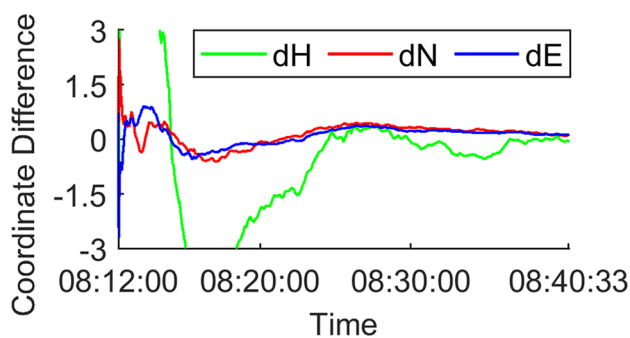

Fig. 10 Height, north, and east coordinate difference over 30 min for the Samsung Galaxy S20. After convergence, the corresponding RMS values are 0.25, 0.30, and 0.24 m, respectively

processing settings. VieVS PPP regularly achieves coordinate convergence times of around 1 min or below with high-quality and high-rate observations by utilizing integer ambiguity fixing. The float solution usually converges within 6–7 min to centimeter-level accuracy. Furthermore, VieVS PPP estimates the ZTD at the centimeter level or below and provides an accurate ionospheric delay estimation in the uncombined model case. Beyond that, the float solution shows a highly stable and precise long-term behavior with up to millimeter accuracy.

Besides high-quality data, raPPPid can handle GNSS observation data from low-cost and smartphone devices. A 2D position accuracy at the meter level or below is achieved with smartphone data after two to three minutes under good conditions. Due to the variable characteristic of GNSS measurements from smartphones, more adaptions and refinements of the observation model are subject to further studies.

Future software developments will focus on improved kinematic data processing, including the Doppler shift into the Kalman Filter and the currently experimental fixing approach in the uncombined model. Extensive tests of raPPPid are still carried out to identify and correct remaining bugs in the software and to improve the robustness of the resulting PPP solutions.

Additional information

Declarations

References

Aichinger-Rosenberger M, Wolf A, Senn C, Hohensinn R, Glaner MF, Moeller G, Soja B, Rothacher M (2023) MPG-NET: a low-cost, multi-purpose GNSS co-location station network for environmental monitoring. Measurement 216:112981. https://doi.org/10.1016/j.measurement.2023.112981

An X, Meng X, Jiang W (2020) Multi-constellation GNSS precise point positioning with multi-frequency raw observations and dual-frequency observations of ionospheric-free linear combination. Satell Navig 1(1):7. https://doi.org/10.1186/s43020-020-0009-x

Bahadur B, Nohutcu M (2018) PPPH: a MATLAB-based software for multi-GNSS precise point positioning analysis. GPS Solut. https://doi.org/10.1007/s10291-018-0777-z

Böhm J, Böhm S, Boisits J, Girdiuk A, Gruber J, Hellerschmied A, Krásná H, Landskron D, Madzak M, Mayer D, McCallum J, McCallum L, Schartner M, Teke K (2018) Vienna VLBI and Satellite Software (VieVS) for Geodesy and Astrometry. PASP 130(986):044503. https://doi.org/10.1088/1538-3873/aaa22b

Boisits J, Glaner M, Weber R (2020) Regiomontan: a regional high precision ionosphere delay model and its application in precise point positioning. Sensors 20(10):2845. https://doi.org/10.3390/s20102845

Chen C, Chang G (2021) PPPLib: An open-source software for precise point positioning using GPS, BeiDou, Galileo, GLONASS, and QZSS with multi-frequency observations. GPS Solut 25(1):18. https://doi.org/10.1007/s10291-020-01052-4

Choy S, Bisnath S, Rizos C (2017) Uncovering common misconceptions in GNSS precise point positioning and its future prospect. GPS Solutions 21(1):13–22. https://doi.org/10.1007/s10291-016-0545-x

Ge M, Gendt G, Rothacher M, Shi C, Liu J (2008) Resolution of GPS carrier-phase ambiguities in precise point positioning (PPP) with daily observations. J Geodesy 82(7):389–399. https://doi.org/10.1007/s00190-007-0187-4

Geng J, Bock Y (2013) Triple-frequency GPS precise point positioning with rapid ambiguity resolution. J Geodesy 87(5):449–460. https://doi.org/10.1007/s00190-013-0619-2

Geng J, Chen X, Pan Y, Mao S, Li C, Zhou J, Zhang K (2019) PRIDE PPP-AR: an open-source software for GPS PPP ambiguity resolution. GPS Solut 23(4):91. https://doi.org/10.1007/s10291-019-0888-1

Glaner M, Weber R (2021) PPP with integer ambiguity resolution for GPS and Galileo using satellite products from different analysis centers. GPS Solut 25(3):102. https://doi.org/10.1007/s10291-021-01140-z

Glaner M (2022) Towards instantaneous PPP convergence using multiple GNSS signals. Dissertation, Vienna University of Technology. https://doi.org/10.34726/hss.2022.73610

Hadas T, Krypiak-Gregorczyk A, Hernández-Pajares M, Kaplon J, Paziewski J, Wielgosz P, Garcia-Rigo A, Kazmierski K, Sosnica K, Kwasniak D, Sierny J, Bosy J, Pucilowski M, Szyszko R, Portasiak K, Olivares-Pulido G, Gulyaeva T, Orus-Perez R (2017) Impact and implementation of higher-order ionospheric effects on precise GNSS applications. J Geophys Res Solid Earth 122(11):9420–9436. https://doi.org/10.1002/2017JB014750

Hernández-Pajares M, Juan JM, Sanz J, Orus R, Garcia-Rigo A, Feltens J, Komjathy A, Schaer SC, Krankowski A (2009) The IGS VTEC maps: a reliable source of ionospheric information since 1998. J Geodesy 83(3–4):263–275. https://doi.org/10.1007/s00190-008-0266-1

Héroux P, Kouba J (1995) GPS precise point positioning with a difference. In: Paper presented at Geomatics '95, Ottawa, Ontario, Canada, 13–15 June

Hofmeister A, Böhm J (2017) Application of ray-traced tropospheric slant delays to geodetic VLBI analysis. J Geod 91(8):945–964. https://doi.org/10.1007/s00190-017-1000-7

Hohensinn R, Stauffer R, Glaner MF, Herrera Pinzón ID, Vuadens E, Rossi Y, Clinton J, Rothacher M (2022) Low-Cost GNSS and real-time PPP: assessing the precision of the u-blox ZED-F9P for kinematic monitoring applications. Remote Sens 14(20):5100. https://doi.org/10.3390/rs14205100

Kouba J, Lahaye F, Tétreault P (2017) Precise point positioning. Springer handbook of global navigation satellite systems. Springer, Cham, pp 723–751

Landskron D, Böhm J (2018a) Refined discrete and empirical horizontal gradients in VLBI analysis. J Geod 92(12):1387–1399. https://doi.org/10.1007/s00190-018-1127-1

Landskron D, Böhm J (2018b) VMF3/GPT3: refined discrete and empirical troposphere mapping functions. J Geod 92(4):349–360. https://doi.org/10.1007/s00190-017-1066-2

Liu W, Shi X, Zhu F, Tao X, Wang F (2019) Quality analysis of multi-GNSS raw observations and a velocity-aided positioning approach based on smartphones. Adv Space Res 63(8):2358–2377. https://doi.org/10.1016/j.asr.2019.01.004

Lou Y, Zheng F, Gu S, Wang C, Guo H, Feng Y (2016) Multi-GNSS precise point positioning with raw single-frequency and dual-frequency measurement models. GPS Solut 20(4):849–862. https://doi.org/10.1007/s10291-015-0495-8

Magnet N (2019) Giomo: a robust modelling approach of ionospheric delays for GNSS real-time positioning applications. Dissertation, Vienna University of Technology. https://doi.org/10.34726/hss.2019.21396

Malys S, Jensen PA (1990) Geodetic point positioning with GPS carrier beat phase data from the CASA UNO experiment. Geophys Res Lett 17(5):651–654

Naciri N, Bisnath S (2021) An uncombined triple-frequency user implementation of the decoupled clock model for PPP-AR. J Geod 95(5):60. https://doi.org/10.1007/s00190-021-01510-y

Pan Z, Chai H, Kong Y (2017) Integrating multi-GNSS to improve the performance of precise point positioning. Adv Space Res 60(12):2596–2606. https://doi.org/10.1016/j.asr.2017.01.014

Pan L, Zhang X, Liu J (2019) A comparison of three widely used GPS triple-frequency precise point positioning models. GPS Solut 23(4):121. https://doi.org/10.1007/s10291-019-0914-3

Petit G, Luzum B (2010) IERS Conventions. IERS Technical Note. (36):179. Verlag des Bundesamts für Kartographie und Geodäsie: Frankfurt am Main, Germany

Schönemann E (2013) Analysis of GNSS raw observations in PPP solutions. Dissertation, Technical University of Darmstadt

Shinghal G, Bisnath S (2021) Conditioning and PPP processing of smartphone GNSS measurements in realistic environments. Satell Navig 2(1):10. https://doi.org/10.1186/s43020-021-00042-2

Suzuki T (2023) Precise position estimation using smartphone raw GNSS data based on two-step optimization. Sensors 23(3):1205. https://doi.org/10.3390/s23031205

Takasu T (2010) Real-time PPP with RTKLIB and IGS real-time satellite orbit and clock. https://gpspp.sakura.ne.jp/paper2005/igsws2010_rtklib.pdf.

Takasu T (2012) PPP ambiguity resolution implementation in RTKLIB v 2.4.2. https://gpspp.sakura.ne.jp/paper2005/ppprtk_201203a.pdf.

Tegedor J, Øvstedal O, Vigen E (2014) Precise orbit determination and point positioning using GPS, Glonass, Galileo and BeiDou. J Geodetic Sci. https://doi.org/10.2478/jogs-2014-0008

Teunissen PJG (1995) The least-squares ambiguity decorrelation adjustment: a method for fast GPS integer ambiguity estimation. J Geodesy 70(1–2):65–82. https://doi.org/10.1007/BF00863419

Teunissen PJG, Montenbruck O (eds) (2017) Springer handbook of global navigation satellite systems. Springer, Cham

Teunissen PJG (2020) GNSS precise point positioning. In: Position, navigation, and timing technologies in the 21st Century. pp 503–528

Wang L, Li Z, Wang N, Wang Z (2021) Real-time GNSS precise point positioning for low-cost smart devices. GPS Solut 25(2):69. https://doi.org/10.1007/s10291-021-01106-1

Wanninger L, Heßelbarth A (2020) GNSS code and carrier phase observations of a Huawei P30 smartphone: quality assessment and centimeter-accurate positioning. GPS Solut 24(2):64. https://doi.org/10.1007/s10291-020-00978-z

Xiao G, Liu G, Ou J, Liu G, Wang S, Guo A (2020) MG-APP: an open-source software for multi-GNSS precise point positioning and application analysis. GPS Solut 24(3):66. https://doi.org/10.1007/s10291-020-00976-1

Zangenehnejad F, Gao Y (2021) GNSS smartphones positioning: advances, challenges, opportunities, and future perspectives. Satell Navig 2(1):24. https://doi.org/10.1186/s43020-021-00054-y

Zangenehnejad F, Jiang Y, Gao Y (2023) GNSS observation generation from smartphone android location API: performance of existing apps. Issues Improv Sens 23(2):777. https://doi.org/10.3390/s23020777

Zhang X, Tao X, Zhu F, Shi X, Wang F (2018) Quality assessment of GNSS observations from an Android N smartphone and positioning performance analysis using time-differenced filtering approach. GPS Solut 22(3):70. https://doi.org/10.1007/s10291-018-0736-8

Zhao C, Zhang B, Zhang X (2021) SUPREME: an open-source single-frequency uncombined precise point positioning software. GPS Solut 25(3):86. https://doi.org/10.1007/s10291-021-01131-0

Zhou F, Dong D, Li W, Jiang X, Wickert J, Schuh H (2018) GAMP: An open-source software of multi-GNSS precise point positioning using undifferenced and uncombined observations. GPS Solut 22(2):33. https://doi.org/10.1007/s10291-018-0699-9

Zumberge JF, Heflin MB, Jefferson DC, Watkins MM, Webb FH (1997) Precise point positioning for the efficient and robust analysis of GPS data from large networks. J Geophys Res 102(B3):5005–5017. https://doi.org/10.1029/96JB03860

Marcus Franz Glaner is a research assistant at the Department of Geodesy and Geoinformation, TU Wien, and received his Ph.D. in 2022. His present research activities focus on satellite navigation, GNSS positioning, and PPP. He is responsible for developing raPPPid, the PPP component of the Vienna VLBI and Satellite Software (VieVS PPP).

Robert Weber is an Associate Professor at the Department of Geodesy and Geoinformation, TU Wien, and former IGS GNSS Working Group chair. His main research includes geodetic reference systems, active GNSS reference station networks, and the application of GNSS for geodynamics and meteorology.